Chapter 9
Terahertz Spectroscopy of Liquids and Biomolecules

D. K. George and A. G. Markelz

Abstract The terahertz regime has particular value for liquid and biomolecular spectroscopy. In the case of liquids, terahertz is sensitive to relaxational and collective motions in liquids [1–13]. Applications include determination of sugar, alcohol, and water content. While there are no narrow band identification features for liquids in the terahertz range, the ability of THz to transmit through packaging materials and high sensitivity of relative water content is considered highly appealing for its use as a method to rapidly verify labeled contents. The determination of the water, sucrose, alcohol, liquid fuel, and petroleum content using terahertz have been demonstrated [1, 10]. The fundamental findings from terahertz measurements of liquids include the hydration number associated with solutes [14, 15], the extent of the perturbation of the liquid structure by the solute [16, 17], and the role of interactions in binary liquids [13, 18] . New collective mode vibrations have been identified for alcohols [19, 20], and the changes in the relaxational dynamics due to mixing, and the role of collective vibrations in ionic liquids [21–24]. In order to achieve these many findings, sensitive measurement techniques and data analysis have been developed. In parallel, great strides in modeling have been made to effectively model the picosecond dielectric response for these highly complex systems.

Biological applications of terahertz have been explored from spectroscopy of biologically relevant molecules as small as sucrose up to organisms such as bacterial spores. Significant progress has been made in fundamental characterization of small biomolecules with accurate modeling of both intramolecular modes, and the intermolecular modes for crystalline material. Initial measurements of small proteins have been explored; however, theoretical understanding is not as well developed. While a variety of groups have demonstrated sensitivity in the THz dielectric response to protein and nucleic acid functional state, the origin of this sensitivity is still some-

D. K. George · A. G. Markelz (✉)
Department of Physics, University at Buffalo, The State University of New York,
New York 14260, USA
e-mail: amarkelz@buffalo.edu

K.-E. Peiponen et al. (eds.), *Terahertz Spectroscopy and Imaging*,
Springer Series in Optical Sciences 171, DOI: 10.1007/978-3-642-29564-5_9,

what controversial.

In this chapter, we will discuss measurement methods, modeling of the terahertz response for these systems, and major results. We will conclude with a discussion on future directions for the applications of terahertz for liquid and biomolecular characterization.

9.1 Liquids

9.1.1 Terahertz Response for Liquids

Typically liquid response is characterized for polar and nonpolar liquids. Let us first look at a listing of some common liquids, the dipole moments for constituent molecules, and the THz absorption coefficient at 3 THz in Table 9.1. We see that water has the largest dipole for those listed, whereas benzene's dipole is zero, and the THz absorption coefficient decreases as the dipole moment decreases [9, 18, 19, 25]. This is a reflection of simplest response of the liquid to the applied electric field, which is simply the dipole alignment following the applied field. There is an effective time for this rotation arising from the bonds (usually weak hydrogen bonds) that must be broken for the molecule to rotate. We refer to this effective alignment time as the relaxation time τ. To calculate the dielectric response arising from this relaxation time we quickly review the relationship between the polarization, displacement field, electric field, electric susceptibility χ and permittivity ε:

$$\begin{aligned} P &= \varepsilon_o \chi E \\ D &= \varepsilon_o \varepsilon_r E = E + P \\ \varepsilon_r &= \varepsilon = 1 + \chi \end{aligned} \tag{9.1}$$

We now develop an expression for the permittivity based on the average time for dipole alignment to the applied field, the Debye relaxation time. The molecular response of the liquid to the applied electric field is split into different components, a fast response polarization P_f, where the polarization follows the field instantaneously, and a slow response polarization P_s:

$$\begin{aligned} P &= P_s + P_f \\ P &= \varepsilon_o(\varepsilon - 1)E \\ P_f &= \varepsilon_o(\varepsilon_\infty - 1)E \end{aligned} \tag{9.2}$$

The rate change of P_s is proportional to the difference between the steady-state polarization and polarization at time t:

Table 9.1

Solvent	Dielectric constant	α(3 THz) (cm^{-1})	Dipole moment (D)
Cyclohexane[a]	2.02	0.3	0.00
Benzene[a]	2.3	4.8	0.00
Chloroform[b]	4.81	7	1.04
1-Propanol[c]	20	35	1.68
Ethanol[c]	24.55	60	1.69
Methanol[c]	33	110	1.70
Water[c]	80	200	1.85

[a]Keiding [b]Cheville et al. [c]Kindt and Schmuttenmaer

$$\frac{\mathrm{d}P_s(t)}{\mathrm{d}t} = \frac{P - (P_f + P_s(t))}{\tau} \tag{9.3}$$

At low frequencies the total polarization will go as the slow susceptibility with

$$\underset{\nu \to 0}{P} = \varepsilon_o(\varepsilon_s - 1)E \tag{9.4}$$

For response at harmonic fields, we substitute $E(t) = E_o \mathrm{e}^{i\omega t}$ and $P_s(t) = P_s \mathrm{e}^{i\omega t}$ into Eq. 9.3

$$\begin{aligned}
E(t) = E_o \mathrm{e}^{i\omega t} &\Rightarrow P_s(t) = P_s \mathrm{e}^{i\omega t} \\
i\omega P_s \mathrm{e}^{i\omega t} &= \frac{\varepsilon_o(\varepsilon_s - 1)E_o \mathrm{e}^{i\omega t} - \varepsilon_o(\varepsilon_\infty - 1)E_o \mathrm{e}^{i\omega t} - P_s \mathrm{e}^{i\omega t}}{\tau} \\
i\omega P_s &= \frac{\varepsilon_o(\varepsilon_s - \varepsilon_\infty)E_o - P_s}{\tau} \\
P_s &= \frac{\varepsilon_o(\varepsilon_s - \varepsilon_\infty)E_o}{1 + i\omega\tau} \\
P &= P_f + P_s \\
\varepsilon_o(\varepsilon - 1)E_o &= \varepsilon_o(\varepsilon_\infty - 1)E_o + \frac{\varepsilon_o(\varepsilon_s - \varepsilon_\infty)E_o}{1 + i\omega\tau} \\
\varepsilon &= \varepsilon_\infty + \frac{(\varepsilon_s - \varepsilon_\infty)}{1 + i\omega\tau}
\end{aligned} \tag{9.5}$$

The dipole alignment may involve the motion of small clusters as well, so that there are often a number of relaxation times. In general the modeling of the dielectric response for liquids and glasses can be written as:

$$\varepsilon(\omega) = \varepsilon_\infty + \sum_i \frac{\Delta\varepsilon_i}{1 + i\omega\tau_i} \tag{9.6}$$

For some liquids, intermolecular coupling can be sufficiently strong so that vibrations between solvent molecules or within a single solvent molecule will also contribute to the dielectric response. These are typically Lorentzian resonances so that a full dielectric response can be modeled as:

$$\varepsilon(\omega) = \varepsilon_\infty + \sum_i \frac{\Delta\varepsilon_i}{1 + i\omega\tau_i} + \sum_j \frac{f(\omega_j)}{(\omega_j^2 - \omega^2) - i\gamma\omega} \tag{9.7}$$

To relate the measured relaxation times and resonant frequencies to the microscopic motions one can calculate the dielectric response using molecular dynamics simulations based on force fields or ab initio calculations. The simulations calculate the trajectories of individual molecules and atoms. One can then calculate the dipole vector for the system for each time step and then determine the dipole–dipole correlation for the system for different times. The dipole–dipole correlation function is related to the product of the absorption coefficient and index by:

$$\alpha(\bar{\nu})n(\bar{\nu}) = \mathrm{Re}\left[\bar{\nu}\{1 - \exp(-\tfrac{hc\bar{(\nu)}}{KT})\} \times \int_{-\infty}^{\infty} \mathrm{d}t \exp(-i2\pi c\bar{\nu}t\langle \mathbf{M}(t)\mathbf{M}(0)\rangle)\right] \tag{9.8}$$

9.1.1.1 Terahertz Measurement Methods for Liquids

The goal in all of these measurements is to characterize the complex permittivity. The most straightforward method for this determination is a transmission measurement using terahertz time domain spectroscopy (THz TDS). This technique is well discussed in previous chapters and a number of commercial systems are now available. For liquid phase measurements, however, the accurate determination of the permittivity is challenged by: accurate determination of the sample thickness, the high absorption for some liquids, and etalon effects. Several techniques have been developed to address these issues.

9.1.2 Liquid Transmission

The simplest method for characterization of a liquid is a transmission measurement. In the UV/Vis and IR ranges standard cuvettes are available for liquid measurements. However, these standard cuvettes are typically made out of materials which strongly attenuate at THz frequencies. In addition, the typical path lengths for standard cells is 5–10 mm. Demountable solution cells with variable spacers are available commercially, an example is shown in Fig. 9.1a. These cells are very flexible in that the window material can be highly transmissive in the FIR, such as zeonor, polyethylene, water free quartz and Teflon, and the spacer can be chosen for optimal sensitivity for the absorbance of material. In Fig. 9.1b the field transmission for the reference and

sample is shown schematically with:

$$t = \frac{E_{\text{sample}}}{E_{\text{reference}}} = \frac{t_{ow}e^{iN_wk_od_w}t_{wo}e^{ik_od_s}t_{ow}e^{iN_wk_od_w}t_{wo}}{t_{ow}e^{iN_wk_od_w}t_{wo}e^{ik_od_s}t_{ow}e^{iN_wk_od_w}t_{wo}} = \frac{t_{ws}t_{sw}}{t_{wo}t_{ow}}e^{i(Ns-1)k_od_s} = \frac{N_S(N_W+1)^2}{(N_W+N_S)^2}e^{i(Ns-1)k_od_s} \tag{9.9}$$

$$t = |t|e^{i\phi} = \frac{N_S(N_W+1)^2}{(N_W+N_S)^2}e^{-\kappa k_od_s}e^{i(n_s-1)k_od_s} \tag{9.10}$$

$$\begin{aligned} |t| &= \frac{n_S(n_W+1)^2}{(n_W+n_S)^2}e^{-\kappa k_od_s} \\ \phi &= (n_s-1)k_od_s \end{aligned} \tag{9.11}$$

where in Eq. 9.9 t_{ij} is the Fresnel transmission coefficient from material i to material j. The subscripts o, w, and s denote atmosphere, window, and sample. In general the THz spectroscopy system is purged of any gas phase water. $N_{S(W)} = n_{S(W)} + i\kappa_{S(W)}$ is the complex index for the sample (window), which has real and imaginary parts. For κ sufficiently small, there is little phase acquired from the Fresnel terms and these can be written in terms of the real parts of the indices. From this then one can immediately determine n_s by inverting the measured phase and then using this determined ns determine κ_s from the magnitude of the transmittance. Equation 9.10 was written without an etalon term. Etalon effects can in many cases be readily removed by simply truncating the transmitted wave before the reflected pulse; however, in some cases samples are too thin to take this approach, as the reflected pulse will overlap the first transmitted pulse. In these cases, the etalon term must be included in the extraction of the optical constants.

$$t = |t|e^{i\phi} = \frac{N_S(N_W+1)^2}{(N_W+N_S)^2}\frac{1-r_{ow}^2e^{i2k_od}}{1-r_{sw}^2e^{i2N_sk_od}}e^{-i\kappa k_od_s}e^{i(n_s-1)k_od_s} \tag{9.12}$$

The most immediate approach to extract $n_s + i\kappa_s$ when etalon is present is to use the measured sample thickness d, window response $n_w + i\kappa_w$, and the measured $|t|$ and ϕ at each frequency and calculate the roots for the coupled equations for $|t|$ and ϕ based on Eq. 9.12 using a standard 2D complex root determination such as is available from Maple or Matlab. For this type of determination one needs to be aware to sufficiently constrain the sampling so that the roots make sense, such as non-negative indices. Regardless of the computation method, this simple method using the transmission through a fixed path length solution cell suffers from the requirements of precise determination of the sample thickness and window dielectric response.

For sufficiently thick samples, the etalon can be avoided by waveform truncation and one does not need to precisely determine sample thickness and window response by using a variable path length cell [6, 17, 24, 26]. Typically, this is achieved by

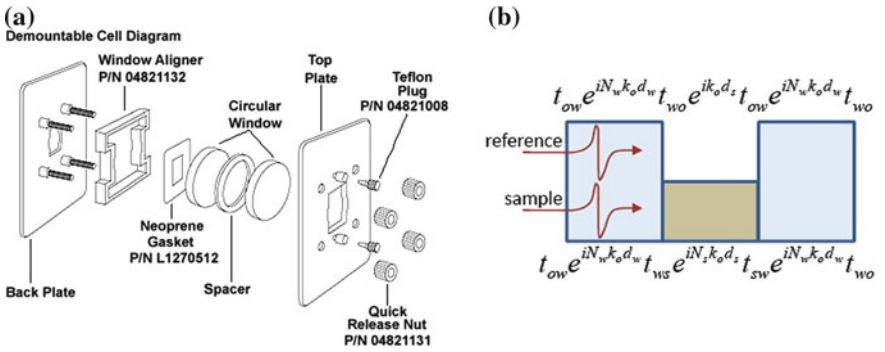

Fig. 9.1 **a** Schematic of commercially available solution cell (Perkin Elmer). **b** Schematic of transmission measurement for a solution cell, with the reference pulses measurement taken for the empty cell and the sample measurement for the liquid filled cell

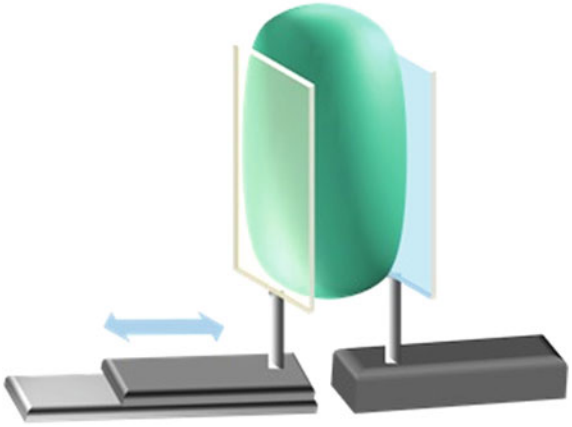

Fig. 9.2 Schematic of a variable path length cell for THz measurements of liquids

placing the liquid in a flexible container, such as a polyethylene bag, and then compressing the bag between two windows, see Fig. 9.2. While absolute thickness determination can be difficult, changes in thickness with an accurate actuator is straightforward. From Eq. 9.4 one can extract the index from a linear fit to the phase as a function of path length variation. Similarly, the imaginary part of the index, κ, can be determined by a linear fit to the $\ln(|t|)$. This method has been used for THz TDS measurements of a wide variety of solvents. However, it is still not ideal for highly absorbing materials, such as water, due to the limited power and dynamic range of typical THz TDS systems. To have a sufficient signal in these cases the path length must be made very thin, with the resulting contamination of the reflected pulse in the main pulse leads to etalon in the transmittance. When this occurs, a simple linear fit cannot be used.

In the case of highly absorbing liquids a number of approaches have been employed. Tunable high power monochromatic sources have been used to achieve

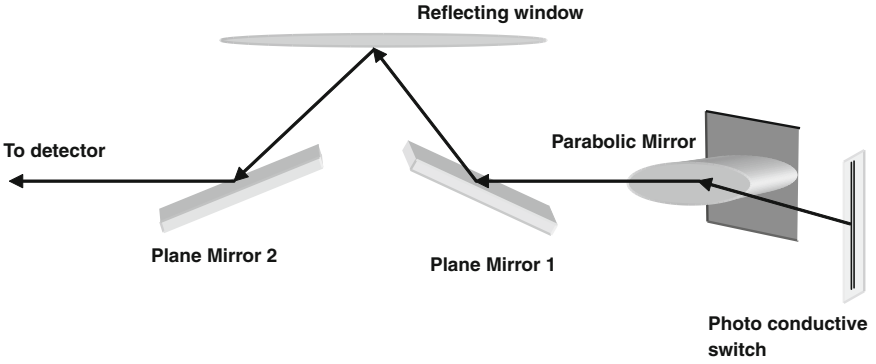

Fig. 9.3 Implementation of reflection THz spectroscopy

high precision permittivity measurements. Xu and coworkers used a free electron laser to characterize the effect of salts on the dielectric response of water, and characterize protein concentration effects for protein-buffer solutions [26, 27]. The output powers for the THz UCSB FELs are 1–15 kW for a 1–6 microsecond pulse width for the MM-FEL and 1–6 kW for 1–20 microsecond pulse width for the FIR-FEL, an approximate factor of 10^7 higher output power than a typical THz TDS system. High power broadband THz TDS systems are becoming more common using tilted phase front or plasma generation. Another highly valuable high power source is the p-Ge laser developed by Bruderman and coworkers [16, 28]. The peak power for the p-Ge laser is 1–10 W; however, similar to the UCSB FEL, these systems are not readily available.

Reflection geometries readily address the dynamic range challenges of highly aborbing materials as the signal is only probing the dielectric interface between a known low loss substrate and the high loss liquid sample [29, 30]. Jepsen group developed the self-referencing geometry for THz TDS, whereas Tanaka group developed ATR geometry more common to IR ATR measurements. In the former method, which is explained in detail below, the liquid lays horizontally on a substrate. The incoming THz light is reflected off the interface between the substrate and liquid. In ATR THz TDS the sample is placed on top of a silicon Dove prism with an apex angle where the is the angle for total internal reflection of THz beam at the sample–prism interface as shown in Fig. 9.4b. The prism is placed at the focus of the THz beam. The beam enters the prism horizontal from one side. Figure 9.3 shows an implementation of reflection THz TDS, while Fig. 9.4a gives a detailed view of the reflection geometry at the sample window, showing the reference and sample beams.

In the self-referencing method, the sample is placed on the upper surface of a horizontal window substrate of appropriate thickness. Based on the refractive index and transmission in the THz region, high purity Si of 1–2 mm thickness is a usual choice. The electric field incident on the bottom surface is partially reflected and partially transmitted. The reflected pulse from the lower surface is used as a reference. The transmitted pulse which passes through the window material again gets partially

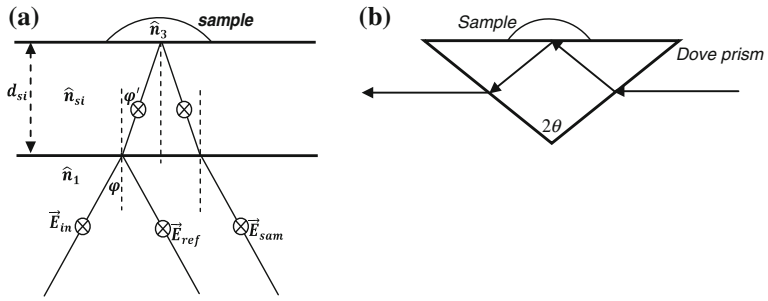

Fig. 9.4 Detailed view of **a** Self-referencing reflection geometry at the silicon window which splits the input THz signal into reference and sample pulses, **b** ATR THz TDS with silicon Dove prism. The sample is placed on top of the window/prism

reflected from the window–sample interface. This pulse which reaches the detector after a time delay carries information about the optical properties of the sample.

In the simplest implementation of transmission THz TDS, which is discussed below, the incident field is purely S-polarized. This can be achieved by the proper orientation of the generating antenna, mirrors, and the window.

The electric field reaching the detector after reflecting off the two interfaces can be represented by the following equations

$$\vec{E}_{\text{ref}} = \hat{r}_{12}\vec{E}_{\text{in}} \tag{9.13}$$

$$\vec{E}_{\text{sam}} = \hat{t}_{12}\hat{r}_{23}\hat{t}_{21}\widehat{E}_{\text{in}}\exp(2i\hat{n}_2 w_2 d_{\text{eff}}/c) \times A_{\text{cal}}\exp(i\Delta_{\text{cal}}) \tag{9.14}$$

$\hat{n_1}, \hat{n_2}, \hat{n_3}$ are the complex refractive indices of the material below the lower surface of the window material and of the sample above the window.

$\vec{E}_{\text{in}}$ the incident electric field, $\vec{E}_{\text{ref}}$ the electric field of the pulse reflected from the lower surface, and $\vec{E}_{\text{sam}}$ the electric field reflected from the window–sample interface. $\hat{r}_{12}$, $\hat{r}_{23}$ are the Fresnel reflection co-efficients at the lower and upper interfaces while $\hat{t}_{12} = \hat{t}_{21}$ is the transmission co-efficient at the lower interface. $A_{\text{cal}}\exp(i\Delta_{\text{cal}})$ represents the calibration factor in amplitude and phase to account for the spatial walk off between reference pulse and the sample pulse. d_{eff} is the effective difference in optical path of the two pulses and is given by

$$\text{d}_{\text{eff}} = \text{d}_{\text{si}}\left(1 - \frac{\sin^2\phi}{n_{\text{si}}^2}\right) \tag{9.15}$$

where $\hat{n}_2 = n_{\text{si}}$ is the refractive index of silicon window material and φ is the angle of incidence

The ratio of the two electric fields is given by

$$\frac{\hat{E}_{\text{sam}}}{\hat{E}_{\text{ref}}} = \frac{\hat{t}_{12}\hat{r}_{23}\hat{t}_{21}}{\hat{r}_{12}} \exp(2in_2w_2d_{\text{eff}}/c) \times A_{\text{cal}} \exp(i\,\Delta_{\text{cal}}) \tag{9.16}$$

Calibration factor can be determined by taking a measurement without the sample (air above the window). In this case $\hat{n}_3 = \hat{n}_{air} = 1$ and

$$A_{\text{cal}} \exp(i\,\Delta_{\text{cal}}) = \frac{\vec{E}^{\text{air}}_{\text{sam}}}{\vec{E}_{\text{ref}}} \cdot \frac{\hat{t}_{12}}{\hat{t}_{12}\hat{r}^{\text{air}}_{23}\hat{t}_{21}} \cdot \exp(-2i\hat{n}_2\omega_2) \tag{9.17}$$

Substituting Eq. 9.17 in Eq. 9.16 yields

$$\frac{\vec{E}_{\text{sam}}}{\vec{E}_{\text{ref}}} = \frac{\hat{r}_{23}}{\hat{r}^{\text{air}}_{23}} \cdot \frac{\vec{E}^{\text{air}}_{\text{sam}}}{\widehat{E}_{\text{sam}}} \tag{9.18}$$

The general equation for Fresnel reflection coefficient at an interface when the incident electric field is purely 's' polarized is given by

$$\hat{r}_s = \frac{n\cos(\varphi) - n'\cos(\varphi)'}{n\cos(\varphi) + n'\cos(\varphi)'} \tag{9.19}$$

Applying Snell's law $n\sin(\varphi) = n'\sin(\varphi')$, we get

$$\hat{r}_s = \frac{n\cos(\varphi) - n'\sqrt{1 - \frac{n^2}{n^2}\sin^{2(\varphi)}}}{n\cos(\varphi) + n'\sqrt{1 - \frac{n^2}{n^2}\sin^{2(\varphi)}}} \tag{9.20}$$

Applying this equation at the window (silicon)—sample interface taking $n_1 = 1$ and using Snell's equation which gives $n_{\text{si}}\sin(\varphi') = n_1\sin(\varphi) = \sin(\varphi)$, we get

$$\hat{r}_{23} = \frac{\sqrt{\hat{n}^2_{\text{si}} - \sin^2\varphi} - \sqrt{\hat{n}^2_3 - \sin^2\varphi}}{\sqrt{\hat{n}^2_{\text{si}} - \sin^2\varphi} + \sqrt{\hat{n}^2_3 - \sin^2(\varphi)}} \tag{9.21}$$

where φ is the angle of incidence at the first interface and the complex index of refraction of the sample Eq. 9.20 can be inverted to obtain $\hat{n}_3 = \hat{n}_{\text{sam}}$;

$$\hat{n}_{\text{sam}} = \frac{\sqrt{(1-\hat{r}_{23})^2 n^2_{\text{si}}} + 4\hat{r}_{23}\sin^2(\varphi)}{1 + \hat{r}_{23}} \tag{9.22}$$

where $\hat{r}_{23}$ can be obtained by inverting equation Eq. 9.17.

For the Tanaka method, more closely related to the standard ATR geometry used in the IR, a dove prism is used, with angles cut to ensure that one can insert the prism into a standard THz path, provided that the Rayleigh range is sufficiently long and

the diameter of the beam sufficiently small. However, in this case one is required to remove the sample for referencing, which may not always be convenient. These reflection techniques have achieved the highest precision in the determination of broadband absorption. Another approach to reflection-type measurements to achieve high sensitivity are waveguide methods [31, 32].

9.1.3 Major Findings and Current Directions

Among the immediate applications of terahertz applied to liquids is the rapid determination of water content in beverages and petroleum samples [1, 2]. This provides a rapid means to determine if the labeled contents are accurate. Other material response has also been characterized such as alkanes and seed oils [8, 33].

A major finding is the extent of the hydration shell for various solutes [16, 28, 34–39]. Here the hydration shell refers to the extent that dynamics of the water surrounding the solute are disrupted from bulk dynamics. Havenith and coworkers have been pioneers in this respect. Agreement has been found with their results by a variety of groups using different techniques. Bonn and coworkers have examined how single ions can disrupt the bulk water hydrogen bond network [15].

A number of groups have also examined the intermolecular coupling for binary liquids. In these studies the THz response is examined as a function of solvent concentration and it has been established that the concentration dependence does not follow a simple effective medium where the net response is fractional sum of the two constituents and that the remaining response arises from the intermolecular coupling. Of particular interest has been ionic liquids [21–24, 40, 41], where a strong change in relaxation time was found for water mixtures, deviating strongly from pure ionic liquids or pure water [24]. Future directions will likely explore the dependence of the disruption of the hydrogen bond network within a polar solvent as a function of the scale of inhomogeneity of hydrophilic and hydrophobic surfaces. In particular, if a critical scale of variation of hydrophobic/hydrophilic surface results in frustration in the hydrogen bond network and a significant change then in the relaxation time.

9.2 Biomolecules

9.2.1 Terahertz Response from Biomolecule

As mentioned in the introduction, THz has been applied to a variety of biological systems. Here we focus on the response from molecular systems as opposed to tissues and organisms. With respect to biomolecular studies we distinguish small biomolecules from macro biomolecules. Small biomolecules include individual nucleotides, glucose, sucrose, individual amino acids, small pharmaceuticals such as ibuprofen

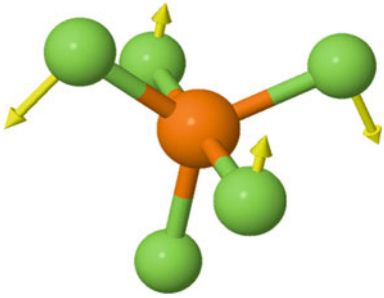

Fig. 9.5 The vector diagram for the 178.95 cm^{-1} E' mode for phosphorus pentafluoride (from the ChemTube site at the University of Liverpool, www.chemtube3d.com/vibrationsPF5.htm)

and chromophores such as hemes and retinal. These molecules have an average of 10–20 atoms/molecule. Vibrations localized to a single or few bonds are in the infrared and vibrations distributed throughout the molecule are in the 50–500 cm^{-1} range. In Fig. 9.5 is shown a vector diagram of the 178.95 cm^{-1} vibrational mode for phosphorus pentafluoride to represent the extended vibration across a small molecule. The mode can be calculated using normal mode analysis (NMA) and the eigenvector for the mode is the 3D displacements for each atom for the given mode. When these small molecules are crystallized, the phonon modes of the crystal will have both an intermolecular and intramolecular component. That is, unlike in the case of simple solids such as NaCl or GaAs, molecular crystals have molecules as the crystal basis and the phonon modes may include both long range correlated motion between molecules and internal motion within the molecular basis.

Biological macromolecules include proteins, polypeptides, DNA, and RNA molecules. Here we further distinguish macromolecules with tertiary structure versus disordered macromolecules that may have some secondary structure elements, but not well-defined tertiary structure. Structural hierarchy for proteins is defined in Fig. 9.6. For example, while DNA chains that are at least 4 nucleotides long will have a double helix structure, longer double helix chains will generally not have well-defined structure, but rather a random coil polymer, similar to the structure in Fig. 9.6a. This will also be true for a variety of polypeptides. Poly-lysine greater than 5 peptides long can have an alpha helix structure (see Fig. 9.6b), but in a solution of 30 % methanol poly-lysine will be in random coil form. Native state proteins however have well-defined tertiary structure. This structure however is not static. Structural motions are essential for protein–protein and protein–ligand interaction. These motions may be correlated or diffusive. A variety of measurements have attempted to measure these motions. Among the methods applied are neutron scattering and X-ray scattering [42–44]. Unfortunately many of these techniques are limited in their ability to truly distinguish between structurally related motions and local diffusive motions. Modeling plays a key role in interpreting the results. Here terahertz studies only now are beginning to have firmer footing [34]. Here we will focus on the simplest approach to understanding the response. It is very likely that this approach will be entirely outdated very soon, as progress in this area is rapid.

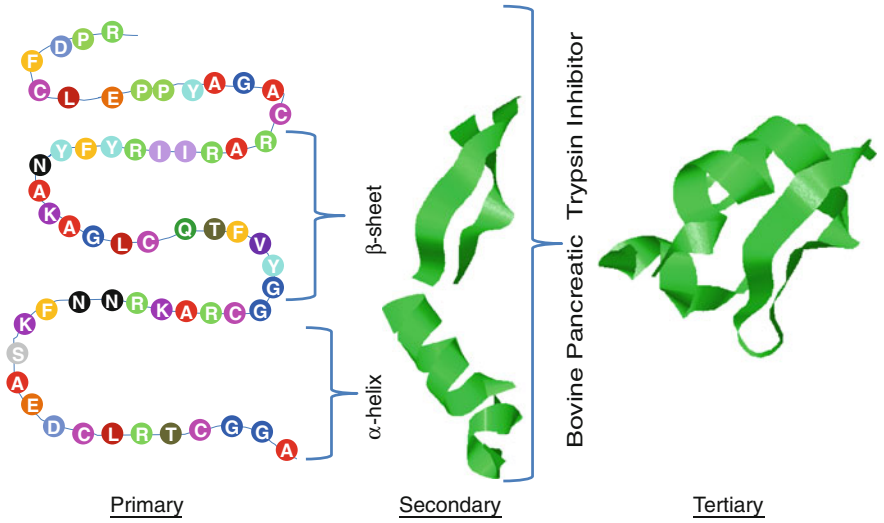

Fig. 9.6 Hierarchy of protein structure shown for bovine pancreatic trypsin inhibitor (BPTI) structure from 1QLQ.pdb. **a** Primary, **b** secondary, **c** tertiary

The simplest approach for protein and RNA response is a full atomic force field calculation. Typically these are done with a variety of molecular mechanics (MM) software. The input to these programs is the protein structure file currently available on the Web from www.pdb.org. The MM software has a database for the molecular force fields and structures associated with amino acids, nucleotides, common salts, solvents, and functional groups (retinal and hemes).

At this writing popular MM programs are CHARMM, AMBER, GROMACS, and NAMD. NAMD and its companion visualization program VMD is available as freeware from the Schulten group (http://www.ks.uiuc.edu/Research/namd/). The procedure to calculate the absorbance is either through NMA, quasiharmoic mode analysis or dipole autocorrelation. The most complete description is to use the dipole autocorrelation as discussed in Sect. 9.1.3. Equation 9.8; however, it is difficult to relate the results to specific motions. The most straightforward method is NMA; however, it is also the least realistic. NMA is the determination of the structural vibrations through evaluation of the effective spring constant by calculating the curvature of the 3N dimensional molecular potential at the energy minimum, where N is the number of atoms in the biomolecule, typically > 300. The process involves first minimizing the potential energy function with respect to the atomic coordinates. The potential energy function is often written in terms for bonding interactions and non-bonding interactions where the potential for the bonding interactions is written as:

$$V(\vec{r}_1, \ldots \vec{r}_N) = \sum_{\text{bonds}} K_b \left(r_{np} - r_{np,o}\right)^2 + \sum_{\text{angles}} K_\theta \left(\theta - \theta_o\right)^2 + \sum_{\text{dihedrals}} K\phi \left(1 + \cos(n\phi - \delta)\right) + \sum_{\text{impropers}} K_\varphi \left(\varphi - \varphi_o\right)^2 + \sum_{\text{Urey-Bradley}} K_{\text{UB}} \left(r_{nl} - r_{nl,o}\right)^2 \tag{9.23}$$

where r_{np} refers to the vector between atoms n and p, θ refers to the angle made by the bonds of three atoms, n, p, and l, and ϕ refers to the dihedral angle made between the two planes of 4 bonded atoms n, p, I and q. Definitions for the improper angles and more detailed definitions can be found in any of the online manuals for the MM programs listed above. As seen this potential is dependent on coefficients for each of the harmonic terms, K_b, K_θ,K_ϕ, and K_{UB}. These coefficients are the force constants and are part of a database associated with the software. The coefficients are in part determined empirically by comparisons of optical measurements with calculated vibrations for small systems. The potential for the non-bonding interactions is written as:

$$\sum_{\text{nonbonded}} \frac{q_n q_p}{4\pi D r_{np}} + \varepsilon_{np} \left[\left(\frac{R_{\min,np}}{r_{np}} \right)^{12} - 2 \left(\frac{R_{\min,np}}{r_{np}} \right)^{6} \right] \tag{9.24}$$

where the first term is the usual long range Coulomb interaction and the second term is the Lennard–Jones potential. This potential energy function can be evaluated for the atomic coordinates for a given protein as downloaded from structure databases; however, the atomic coordinates substituted into Eq. 9.23 and 9.24 will not in general give the minimized energy. The coordinates for the minimized energy are small deviations from the measured structures. These coordinates are determined through a standard energy minimization process. Once the coordinates of the energy minimized structure are determined one can apply the harmonic approximation to attain effective force constants, eigenfrequencies and eigenvectors for structural vibrations. For small perturbations about the minimum one can then use a harmonic approximation of the potential and thus determine the eigenfrequencies from the curvature of the potential. In one dimension we have:

$$V(x) = V(x_0) + \frac{\mathrm{d}V}{\mathrm{d}x}\Big|_{x=x_o} (x - x_o) + \frac{1}{2} \frac{\mathrm{d}^2 V}{\mathrm{d}x^2}\Big|_{x=x_o} (x - x_o)^2 + \cdots \tag{9.25}$$

At the potential minimum

$$\frac{\mathrm{d}V}{\mathrm{d}x}\Big|_{x=x_o} = 0$$

$$V(x) \sim V(x_o) + \frac{1}{2} \frac{\mathrm{d}^2 V}{\mathrm{d}x^2}\Big|_{x=x_o} (x - x_o)^2 = V(x_o) + \frac{1}{2} k (x - x_o)^2 \tag{9.26}$$

$$\omega = \sqrt{\frac{k}{m}}$$

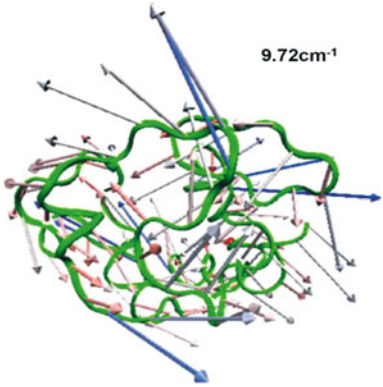

Fig. 9.7 Vector diagram for the 9.72 cm^{-1} quasi harmonic mode for oxidized cytochrome c (from Yunfen He et. al. Biophys. J. 100, 1058 (2010))

For these very large systems, to determine the eigenfrequencies and eigenvectors the 3N × 3N mass weighted Hessian matrix is diagonalized, where the elements of the matrix are:

$$H_{nipj} = \frac{\frac{\partial^2 V}{\partial n_i \partial p_j}}{\sqrt{m_n}\sqrt{m_p}} \tag{9.27}$$

where *n* ,*p* refer to specific atoms and *i, j* refer to *x,y,z* coordinate of that atom. In Fig. 9.7 we show an eigenmode for cytochrome c. The vectors for the mode are drawn somewhat similar to those for the small molecule in Fig. 9.5; where the displacement vector associated with the vibration is shown for each atom however, for the protein with >300 atoms such a representation would be unilluminating. Instead, the atomic displacements are averaged about the alpha carbon of a given peptide and the net displacement for the average is plotted on the alpha carbon. In the terahertz range, the number of modes *I* is very high and the modes are closely spaced together, with typical mode spacing for frequencies below 100 cm^{-1} (3 THz) of $< 0.5\,cm^{-1}$. Measurement on small molecules have shown that internal vibrational resonances have linewidths typically greater than 5 cm^{-1} at room temperature; thus, it is somewhat justified to evaluate an effective density of states through the histogram of the evaluated eigenfrequencies with bin size ∼5 cm^{-1}. Figure 9.8a shows the evaluated density of states for NMA using this approach. To determine the light absorption from NMA one uses the "double harmonic" approximation, where the light absorbance is related to the dipole derivative associated with a particular eigenmode.

For mode frequency ν_k, the integrated intensity Γ_k has units of molar absorptivity and is proportional to the absorption coefficient [45]. We draw a distinction of Γ_k with the often calculated absorption intensity, A_k. A_k differs from Γ_k by a factor of ν_k and is not directly related to the derivation of the absorption coefficient from Fermi's Golden rule. The double harmonic approximation consists of modes calculated from a harmonic expansion of the potential and an approximation of the dipole moment inner product using the quadratic term in the Taylor expansion of the dipole. Γ can be obtained from the dipole derivatives calculated from the quasiharmonic analysis

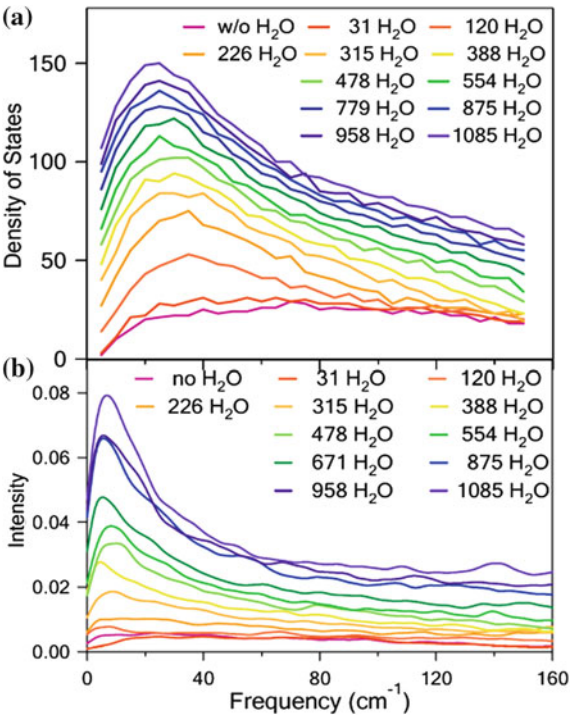

Fig. 9.8 Normal mode analysis calculations for reduced cytochrome as a function of hydration. **a** Vibrational density of states, **b** absorbance intensity

using [46]:

$$\Gamma_k = \frac{N_0 \pi^2}{3c^2 \varepsilon_0 \omega_k} \left(\frac{\partial p}{\partial Q_k} \right)^2 \tag{9.28}$$

where ε_0 is the permittivity of vacuum, and N_0 is the Avogadro number and the magnitude of the dipole derivative

The net calculated absorption coefficient is proportional to the sum of Lorentzian oscillators with relaxation rates γ such that we define our quasi harmonic calculated absorption coefficient as

$$\alpha_{\mathrm{QH}}(\omega) = \sum_k \frac{1}{\pi} \frac{\Gamma_k \gamma^2}{(\omega - \omega_k)^2 + \gamma^2} \tag{9.29}$$

Figure 9.8b shows the calculated absorbance using the double harmonic approximation for cytochrome c. While the absorbance calculated in this way does resemble the measured absorbance, unfortunately there are a number of serious flaws to the NMA approach. First the calculation is at zero temperature and second it completely neglects the anharmonicity in the potential. As to the accurate prediction of the terahertz response, it has actually failed a number of tests with respect to correctly

calculating the frequency, hydration, and oxidation dependence. The flaw lies in that while these large-scale vibrations will contribute to the terahertz signal, they do not constitute the entire biomolecular terahertz response. In addition, rotational motions of the surface side chains and solvent will contribute to absorption at these frequencies. Nevertheless, the main prediction of these MM calculations that large-scale correlated motions occur in proteins at terahertz frequencies may be qualitatively correct. Rheinstädter and coworkers have found using inelastic neutron scattering on 2D bacteriorhodopsin protein lattice an optical phonon mode at 3.6 cm^{-1} [42].

9.2.1.1 Terahertz Measurements Methods for Biomolecules: Solid State Measurements

For the microcrystalline small biomolecules, transmission measurements on pressed pellets can be performed. However, Rayleigh scattering will broaden the measured resonances. Nevertheless, measurements on pressed pellets have demonstrated that the THz spectroscopy can distinguish between different isomers. In general the absorption coefficient for these materials is 10-50 cm^{-1}; thus, to remain within the dynamic range of typical THz TDS systems pressed pellets of pure material should be no more than 100 micron thick. It is difficult to form and easily handle such thin pellets. In addition, these thicknesses will introduce etalon effects which will obscure the observation of crystal mode absorbance lines. To overcome this, low absorbance filler material is used, usually polyethylene (PET), although Teflon has also been used frequently. This method of mixing the crystalline powder sample in with filler is sometime referred to as embedding the sample in a matrix. Care should be taken to have uniform mixing of the sample with the filler. A lack of uniform mixing of the sample with the PET can result in apparent resonances due to spatial variation in the frequency content of that the terahertz focus. Often pharmaceutical tablets have THz transparent fillers so measurement of these can be made directly. The filler should have low frequency-independent absorbance over the range of measurement. For small biomolecules, sucrose, lactose, etc., generally form small crystallites and do not require hydration for structural uniformity. Proteins can also be in powder form, also known as lyophilized or freeze dried. A key problem in comparing results from different proteins from different groups is the determination of absolute absorbance. Because pellets often include filler and the pressures used are not uniform, the densities vary and thus the absorption coefficient may not be comparable group to group. In these solid phase measurements we see no distinct features, but rather a glass-like response.

For high precision measurements, extremely sensitive measurement can be performed using a waveguide technique [47]. Here crystalline films are grown on the plates forming the waveguide walls. The samples are necessarily highly uniform. Authors have demonstrated that the results are independent of wall material and a wide variety of materials readily form crystallites on the waveguide walls. However, protein crystallization can be difficult under even highly controlled conditions, so

the waveguide method may not be readily applicable to protein and polynucleotide measurements.

Comparison of these results with calculations is somewhat compromised by the fact that the samples are freeze-dried proteins, which often do not have native state structure. Fully hydrated proteins will have native structure. So it would seem essential that THz measurements be performed with hydrated samples. There are several approaches to achieve these. One is to use films that are hydrated. A second approach is to use liquid phase samples. Films can be formed by dropping solution on substrates and drying. In general, the substrates must be hydrophilic and drying should be controlled to ensure a final uniform thickness. For measurements, the films transmission is normalized to the bare substrate and the sample is held in a hydration controlled cell. Hydration control can be achieved by circulating air over a saturated salt solution or from a dew point generator and pumping this hydrated air through the hydration cell containing the sample. Hydration controlled measurement have found a rapid increase in absorbance for myoglobin and hen egg white lysozyme at 30 % by weight water to protein, whereas the change in THz absorbance with hydration suddenly decreases with cytochrome c at this same hydration [48–50]. This change in protein dynamics with hydration is interesting and certainly should be explored further. Hydrate film measurements are limited by the ability to make uniform films and the requirements of controlled humidity. Liquid phase measurements are preferable for sample uniformity.

9.2.1.2 Terahertz Measurements Methods for Biomolecules: Liquid Phase Measurements

The most direct method to ensure uniformity and native state structure for protein and polynucleotides is solution phase measurements. However, given that the powder pellet measurements indicate that the absorption coefficient of most dried proteins at 1 THz is $\sim 10\,\mathrm{cm}^{-1}$ and the liquid water absorbance at the same frequency is $\sim 200\,\mathrm{cm}^{-1}$, the main effect one sees at room temperature is a decrease in absorbance with increasing protein concentration due to the displacement of the highly absorbing water. However, high precision measurements have shown that the concentration dependence is not a simple linear decrease in absorbance with increasing protein concentration, but rather as the concentration increases, the decrease in absorbance slows and then decreases again more rapidly above a critical concentration. The explanation of this effect has been that the terahertz permittivity of the solvent immediately adjacent to the protein surface is altered by the interaction with the protein and this perturbation extends into the liquid [28, 36, 37]. The extent of the perturbed solvent is referred to the solvation shell. Through precise measurements it has been estimated that the solvation shell extends $\sim 20\,\text{Å}$ from the protein surface and that the terahertz absorbance is higher from the solvation shell water than from bulk water. At high enough concentrations (>5 mg/ml), these hydration shells overlap and no bulk water should be present. The typical protein concentration within a cell is >200 mg/ml, indicating that in the cellular environment all water is

associated with the solvation shells and no bulk water is present; thus, THz measurements of such high concentration solutions are both reasonable biologically and somewhat easier to perform than pellets or hydrated films. In addition, the solvation water appears to have similar temperature dependence as bulk water, with the absorption due to water dropping significantly below 273 K, the freezing point of water. This decrease in absorbance arises from the rotational motions in liquid water slowing down, with the relaxational loss moving to the MHz range. Finally, solution phase measurements also allow one to perform standard assays on the samples used for terahertz studies to confirm native state conformation and functional state such as ligand binding or oxidation. This is essential if one is to be certain that the samples are homogeneous and relevant. For example, fluorescence measurements are often used to confirm binding and UV circular dichroism measurements are used to verify secondary and tertiary structure. Groups have begun to use this method to determine the role of secondary structure in terahertz response, sensitivity to ligand binding, and the structural dependence of the protein dynamical transition [51, 52]. Figure 9.9 shows the measurements done in this way for lysozyme when it is unbound and bound to a small ligand, triacetyl glucosamine (3NAG).

9.2.1.3 Terahertz Measurements Methods for Biomolecules: Crystal Phase Measurements

As protein crystals are generally more than 50 % water by weight, they offer a somewhat ideal form for optical measurements. The molecular alignment in crystals offers the possibility of polarization selection of the optically excited modes. Unfortunately these measurements are still somewhat challenging and only one group has successfully performed them at this writing [53]. The main challenge for these measurements is the limitation in the terahertz diffraction limited spot size, which then requires large crystals (∼2 mm).

9.2.2 Major Findings and Current Directions

Terahertz measurements of proteins and protein solutions have already made a large impact on outstanding scientific questions. The most profound to date are the determination of the extent of the solvation water and the determination of the origin of the so-called protein dynamical transition. The protein dynamical transition is generally associated with a rapid increase in the average root mean squared atomic displacement for the protein at ∼220 K. The imaginary part of the terahertz permittivity has this same rapid increase with temperature. Through THz measurements it has been established that the rapid change is not associated with protein structure, but in fact is seen down to very small peptides. These measurements suggest that the 220 K transition is possibly an indication of thermally activated collective motion of the adjacent solvent, and the size dependence for the occurrence of the transition

indicates the length scale of the collective excitation of the solvent. Overall THz measurement of protein do not indicate narrowband features; there have been a few exceptions to this [54, 55]. The key issue is that the correlated structural motions discussed in the beginning of this section account for only a small part of the dielectric response. Diffuse motion and librational (constrained rotational) motions will constitute the main THz absorbance for these samples. Nevertheless, there are a number of intriguing results from a wide variety of groups that suggest THz is sensitive to protein structure and binding state.

A variety of groups have examined if the THz response changes with protein denaturing. Because of the special sample requirements for terahertz measurements, (low water content or frozen solutions) comparison between different groups needs to be carefully considered. Results for lyophilized samples is the most suspect, as lyophilization itself is a cause of partial denaturing. Further the method used to denature a sample will determine the overall final morphology of the sample. For example, at high protein concentrations, denaturing by pH or thermally will result in disruption of structural bonds and these unprotected groups are free to cross bind between different random coil proteins. This cross- linking can result in the formation of a gel. In general, gels have a lower THz response than the native state samples. The THz absorbance decreases further with increasing aggregation and cross-linking as discussed by Abbott and coworkers in the case of lacto globulin [56]. This decrease in THz response with thermal denaturing was seen also for bovine serum albumin [57]. However, in the case of denaturing by guanidine hydrochloride and urea, the denaturant replaces the structural peptide–peptide bonding, protecting the random coil from interaction with adjacent denatured proteins, preventing gel formation. Terahertz measurements on GdnHCl denatured proteins have found an increase in THz response relative to native state. Measurement of the pure solvent with denaturant have shown that the increase with denaturing does not arise from the absorbance of the denaturant. It is likely that the increased exposure of peptide side changes to the solvent may play a role in the increase of librational contribution to the THz loss [58, 59].

While there have been a number of other interesting studies such as sensitivity to amyloid fibrillation [60], we will discuss only one other common observation to date and that is THz sensitivity to protein ligand binding. A number of groups have considered the binding between biotin and strepavidin [61, 62]. The binding is so strong that it is considered an essential test for any candidate binding assay. Terahertz absorbance increases with binding consistently. Another classic demonstration of THz sensitivity to binding is DNA hybridization [63]. It again has been shown consistently that THz response increases with DNA hybridization. Finally, for small ligand binding to hinge bending proteins, it has been demonstrated that the terahertz response decreases with binding [52]. These consistent results of THz sensitivity to protein binding have not been thoroughly explored. The size of the response, in particular the change in the refractive index with binding, if far in excess the change used for surface plasmon detection. These early results strongly motivate the further exploration of THz response for biological systems.

References

1. P.U. Jepsen, U. Moller, H. Merbold, Investigation of aqueous alcohol and sugar solutions with reflection terahertz time-domain spectroscopy. Opt. Express **15**(22), 14717–14737 (2007)
2. U. Moller, D.G. Cooke, K. Tanaka, P.U. Jepsen, Terahertz reflection spectroscopy of Debye relaxation in polar liquids [Invited]. J. Opt. Soc. Am. B Opt. Phys. **26**(9), A113–A125 (2009)
3. Y. Yomogida, Y. Sato, R. Nozaki, T. Mishina, J. Nakahara, Comparative dielectric study of monohydric alcohols with terahertz time-domain spectroscopy. J. Mol. Struct. **981**(1–3), 173–178 (2010)
4. Y. Yomogida, Y. Sato, R. Nozaki, T. Mishina, J. Nakahara, Comparative study of boson peak in normal and secondary alcohols with terahertz time-domain spectroscopy. Phys. B Condens. Matter **405**(9), 2208–2212 (2010)
5. Y. Danten, M. Besnard, J.C. Delagnes, P. Mounaix, Far infrared absorption and terahertz time domain spectroscopy of liquid CS2: experiments and molecular dynamics simulation. Appl. Phys. Lett. **92**(21), 214102 (2008)
6. J.T. Kindt, C.A. Schmuttenmaer, Far-infrared dielectric properties of polar liquids probed by femtosecond terahertz pulse spectroscopy. J. Phys. Chem. **100**(24), 10373–10379 (1996)
7. J.P. Laib, D.V. Nickel, D.M. Mittleman, Terahertz vibrational modes induced by heterogeneous nucleation in n-alkanes. Chem. Phys. Lett. **493**(4–6), 279–282 (2010)
8. J.S. Li, X.J. Li, Determination principal component content of seed oils by THz-TDS. Chem. Phys. Lett. **476**(1–3), 92–96 (2009)
9. S.R. Keiding, Dipole correlation functions in liquid benzenes measured with terahertz time domain spectroscopy. J. Phys. Chem. A **101**(29), 5250–5254 (1997)
10. Y.S. Jin, G.J. Kim, C.H. Shon, S.G. Jeon, J.I. Kim, Analysis of petroleum products and their mixtures by using terahertz time domain spectroscopy. J. Korean Phys. Soc. **53**(4), 1879–1885 (2008)
11. J.P. Laib, D.M. Mittleman, Temperature-dependent terahertz spectroscopy of liquid n-alkanes. J. Infrared Millim. Terahertz Waves **31**(9), 1015–1021 (2010)
12. P. Dutta, K. Tominaga, Dependence of low frequency spectra on solute and solvent in solutions studied by terahertz time-domain spectroscopy. Mol. Phys. **107**(18), 1845–1854 (2009)
13. A. Oka, K. Tominaga, Terahertz spectroscopy of polar solute molecules in non-polar solvents. J. NonCryst. Solids **352**(42–49), 4606–4609 (2006)
14. T. Arikawa, M. Nagai, K. Tanaka, Characterizing hydration state in solution using terahertz time-domain attenuated total reflection spectroscopy. Chem. Phys. Lett. **457**(1–3), 12–17 (2008)
15. K.J. Tielrooij, N. Garcia-Araez, M. Bonn, H.J. Bakker, Cooperativity in ion hydration. Science **328**(5981), 1006–1009 (2010)
16. U. Heugen, G. Schwaab, E. Brundermann, M. Heyden, X. Yu, D.M. Leitner, M. Havenith, Solute-induced retardation of water dynamics probed directly by terahertz spectroscopy. Proc. Natl. Acad Sci. U. S. A. **103**, 12301–12306 (2006)
17. J. Xu, K.W. Plaxco, S.J. Allen, J.E. Bjarnason, E.R. Brown, 0.15–3.72 THz absorption of aqueous salts and saline solutions. Appl. Phys. Lett. **90**(3), 031908 (2007)
18. B.N. Flanders, R.A. Cheville, D. Grischkowsky, N.F. Scherer, Pulsed terahertz transmission spectroscopy of liquid CHCl3, CCl4, and their mixtures. J. Phys. Chem. **100**(29), 11824–11835 (1996)
19. Y. Yomogida, Y. Sato, R. Nozaki, T. Mishina, J. Nakahara, Comparative dielectric study of monohydric alcohols with terahertz time-domain spectroscopy. J. Mol. Struct. **981**(1–3), 173–178 (2010)
20. Y. Yomogida, Y. Sato, R. Nozaki, T. Mishina, J. Nakahara, Comparative study of boson peak in normal and secondary alcohols with terahertz time-domain spectroscopy. Phys. B Condens. Matter **405**(9), 2208–2212 (2010)
21. K. Yamamoto, M. Tani, M. Hangyo, Terahertz time-domain spectroscopy of imidazolium ionic liquids. J. Phys. Chem. B **111**(18), 4854–4859 (2007)

22. Y. Shim, H.J. Kim, Dielectric relaxation, ion conductivity, solvent rotation, and solvation dynamics in a room-temperature ionic liquid. J. Phys. Chem. B **112**(35), 11028–11038 (2008)
23. J. Sangoro, C. Iacob, A. Serghei, S. Naumov, P. Galvosas, J. Karger, C. Wespe, F. Bordusa, A. Stoppa, J. Hunger, R. Buchner, F. Kremer, Electrical conductivity and translational diffusion in the 1-butyl-3-methylimidazolium tetrafluoroborate ionic liquid. J. Chem. Phys. **128**(21), 214509 (2008)
24. M. Koeberg, C.C. Wu, D. Kim, M. Bonn, THz dielectric relaxation of ionic liquid: water mixtures. Chem. Phys. Lett. **439**(1–3), 60–64 (2007)
25. J.T. Kindt, C.A. Schmuttenmaer, Far-infrared dielectric properties of polar liquids probed by femtosecond terahertz pulse spectroscopy. J. Chem. Phys. **100**(24), 10373 (1996)
26. J. Xu, K.W. Plaxco, S.J. Allen, Probing the collective vibrational dynamics of a protein in liquid water by terahertz absorption spectroscopy. Protein Sci. **15**(5), 1175–1181 (2006)
27. J. Xu, K.W. Plaxco, S.J. Allen, Collective dynamics of lysozyme in water: terahertz absorption spectroscopy and comparison with theory. J. Phys. Chem. B **110**(47), 24255–24259 (2006)
28. S. Ebbinghaus, S.J. Kim, M. Heyden, X. Yu, U. Heugen, M. Gruebele, D.M. Leitner, M. Havenith, An extended dynamical hydration shell around proteins. Proc. Natl. Acad Sci. U. S. A. **104**(52), 20749–20752 (2007)
29. M. Nagai, H. Yada, T. Arikawa, K. Tanaka, Terahertz time-domain attenuated total reflection spectroscopy in water and biological solution. Int. J. Infrared Millim. Waves **27**(4), 505–515 (2006)
30. H. Hirori, K. Yamashita, M. Nagai, K. Tanaka, Attenuated total reflection spectroscopy in time domain using terahertz coherent pulses. Jpn. J. Appl. Phys. Part 2 Lett. Express Lett. **43**(10A), L1287–L1289 (2004)
31. B. You, T.A. Liu, J.L. Peng, C.L. Pan, J.Y. Lu, A terahertz plastic wire based evanescent field sensor for high sensitivity liquid detection. Opt. Express **17**(23), 20675–20683 (2009)
32. L. Cheng, S. Hayashi, A. Dobroiu, C. Otani, K. Kawase, T. Miyazawa, and Y. Ogawa, Terahertz-wave absorption in liquids measured using the evanescent field of a silicon waveguide. Appl. Phys. Lett. **92**(18), 181104 (2008)
33. J.P. Laib, D.V. Nickel, D.M. Mittleman, Terahertz vibrational modes induced by heterogeneous nucleation in n-alkanes. Chem. Phys. Lett. **493**(4–6), 279–282 (2010)
34. M. Heyden, J. Sun, S. Funkner, G. Mathias, H. Forbert, M. Havenith, D. Marx, Dissecting the THz spectrum of liquid water from first principles via correlations in time and space. Proc. Natl. Acad. Sci. U. S. A. **107**(27), 12068–12073 (2010)
35. D.A. Schmidt, O. Birer, S. Funkner, B.P. Born, R. Gnanasekaran, G.W. Schwaab, D.M. Leitner, M. Havenith, Rattling in the cage: ions as probes of sub-picosecond water network dynamics. J. Am. Chem. Soc. **131**(51), 18512–18517 (2009)
36. S.J. Kim, B. Born, M. Havenith, M. Gruebele, Real-time detection of protein-water dynamics upon protein folding by terahertz absorption. Angewandte Chemie Int. Ed. **47**(34), 6486–6489 (2008)
37. S. Ebbinghaus, S.J. Kim, M. Heyden, X. Yu, M. Gruebele, D.M. Leitner, M. Havenith, Protein sequence- and pH-dependent hydration probed by terahertz spectroscopy. J. Am. Chem. Soc. **130**(8), 2374–2375 (2008)
38. M. Sajadi, Y. Ajaj, I. Ioffe, H. Weingartner, N.P. Ernsting, Terahertz absorption spectroscopy of a liquid using a polarity probe: a case study of trehalose/water mixtures. Angew. Chem. Int. Ed. **49**, 454–457 (2010)
39. M.L.T. Asaki, A. Redondo, T.A. Zawodzinski, A.J. Taylor, Dielectric relaxation of electrolyte solutions using terahertz transmission spectroscopy. J. Chem. Phys. **116**(19), 8469–8482 (2002)
40. M. Krüger, E. Bründermann, S. Funkner, H. Weingärtner, M. Havenith, Communications: polarity fluctuations of the protic ionic liquid ethylammonium nitrate in the terahertz regime. J. Chem. Phys. **132**, 101101 (2010)
41. A. Chakraborty, T. Inagaki, M. Banno, T. Mochida, K. Tominaga, Low-frequency spectra of metallocenium ionic liquids studied by terahertz time-domain spectroscopy. J. Phys. Chem. A **115**, 1313–1319 (2011)

42. M.C. Rheinstadter, K. Schmalzl, K. Wood, D. Strauch, Protein–protein interaction in purple membrane. Phys. Rev. Lett. **103**(12), 128104 (2009)
43. K. Wood, C. Caronna, P. Fouquet, W. Haussler, F. Natali, J. Ollivier, A. Orecchini, M. Plazanet, G. Zaccai, A benchmark for protein dynamics: Ribonuclease A measured by neutron scattering in a large wavevector-energy transfer range. Chem. Phys. **345**, 305–314 (2008)
44. D. Liu, X.-q. Chu, M. Lagi, Y. Zhang, E. Fratini, P. Baglioni, A. Alatas, A. Said, E. Alp, S.-H. Chen, Studies of phononlike low-energy excitations of protein molecules by inelastic X-ray scattering. Phys. Rev. Lett. **101**, 135501 (2008)
45. W.B. Person, G. Zerbi, *Vibrational Intensities in Infrared and Raman Spectroscopy*. (Elsevier Scientific Publishing, Amsterdam, 1982)
46. B.S. Galabov, T. Dudev, *Vibrational Intensities* (Elsevier Science, Amsterdam, 1996)
47. J.S. Melinger, N. Laman, S.S. Harsha, S. Cheng, D. Grischkowsky, High-resolution waveguide terahertz spectroscopy of partially oriented organic polycrystalline films. J. Phys. Chem. A **111**, 10977–10987 (2007)
48. C.F. Zhang, S.M. Durbin, Hydration-induced far-infrared absorption increase in myoglobin. J. Phys. Chem. B **110**(46), 23607–23613 (2006)
49. J. Knab, J.-Y. Chen, A. Markelz, Hydration dependence of conformational dielectric relaxation of lysozyme. Biophys. J. **90**, 2576–2581 (2006)
50. Y.F. He, J.Y. Chen, J.R. Knab, W.J. Zheng, A.G. Markelz, Evidence of protein collective motions on the picosecond timescale. Biophys. J. **100**(4), 1058–1065 (2011)
51. T. Ding, R.Y. Li, J.A. Zeitler, T.L. Huber, L.F. Gladden, A.P.J. Middelberg, R.J. Falconer, Terahertz and far infrared Spectroscopy of alanine-rich peptides having variable ellipticity. Opt. Express **18**(26), 27431–27444 (2010)
52. J.Y. Chen, J.R. Knab, S.J. Ye, Y.F. He, A.G. Markelz, Terahertz dielectric assay of solution phase protein binding. Appl. Phys. Lett. **90**(24), 243901 (2007)
53. K.M. Tych, A.D. Burnett, C.D. Wood, J.E. Cunningham, A.R. Pearson, A.G. Davies, E.H. Linfield, Applying broadband terahertz time-domain spectroscopy to the analysis of crystalline proteins: a dehydration study. J. Appl. Crystallogr. **44**, 129–133 (2011)
54. E.R. Brown, E.A. Mendoza, D.Y. Xia, S.R.J. Brueck, Narrow THz spectral signatures through an RNA solution in nanofluidic channels. IEEE Sens. J. **10**(3), 755–759 (2010)
55. Y.W. Sun, Y.T. Zhang, E. Pickwell-MacPherson, Investigating antibody interactions with a polar liquid using terahertz pulsed spectroscopy. Biophys. J. **100**(1), 225–231 (2011)
56. G.M. Png, R.J. Falconer, B.M. Fischer, H.A. Zakaria, S.P. Mickan, A.P.J. Middelberg, D. Abbott, Terahertz spectroscopic differentiation of microstructures in protein gels. Opt. Express **17**(15), 13102–13115 (2009)
57. H. Yoneyama, M. Yamashita, S. Kasai, K. Kawase, R. Ueno, H. Ito, T. Ouchi, Terahertz spectroscopy of native-conformation and thermally denatured bovine serum albumin (BSA). Phys. Med. Biol. **53**(13), 3543–3549 (2008)
58. H. Chen, L. Wang, Y.G. Qu, T.Y. Kuang, L.B. Li, W.X. Peng, Investigation of guanidine hydrochloride induced chlorophyll protein 43 and 47 denaturation in the terahertz frequency range. J. Appl. Phys. **102**(7) 74700 (2007)
59. Y. He, P.I. Ku, J.R. Knab, J.-Y. Chen, A.G. Markelz, Protein dynamical transition does not require protein structure. Phys. Rev. Lett. **101**, 178103 (2008)
60. R. Liu, M.X. He, R.X. Su, Y.J. Yu, W. Qi, Z.M. He, Insulin amyloid fibrillation studied by terahertz spectroscopy and other biophysical methods. Biochem. Biophys. Res. Commun. **391**(1), 862–867 (2010)
61. Y. Ogawa, S. Hayashi, M. Oikawa, C. Otani, K. Kawase, Interference terahertz label-free imaging for protein detection on a membrane. Opt. Express **16**(26), 22083–22089 (2008)
62. A. Menikh, S.P. Mickan, H. Liu, R. MacColl, X.-C. Zhang, Label-free amplified bioaffinity detection using terahertz wave technology. Biosens. Bioelectron. **20**(3), 658–662 (2004)
63. M. Brucherseifer, M. Nagel, P.H. Bolivar, H. Kurz, A. Bosserhoff, R. Buttner, Label-free probing of the binding state of DNA by time-domain terahertz sensing. Appl. Phys. Lett. **77**(24), 4049–4051 (2000)